Internet-Based Smart-Space Navigation of a Car-Like Wheeled Robot Using Fuzzy-Neural Adaptive Control

Chih-Lyang Hwang, *Member, IEEE*, and Li-Jui Chang

***Abstract*—In this paper, a navigation system is developed. The system includes path tracking and obstacle avoidance apparatus for a car-like wheeled robot (CLWR) within an Internet-based smart-space (IBSS) using fuzzy-neural adaptive control (FNAC). Two distributed charge-coupled device (CCD) cameras are installed to capture both the dynamic pose of the CLWR and the obstacle. Based on the control authority of these two CCD cameras, a suitable reference command that contains the desired steering angle and angular velocity for the FNAC built into the client computer is planned. Because of the delay encountered by the transmission through the Internet network (IN) and the wireless local area network (WLAN) and the nonlinear coupling features of the CLWR, a weighted combination of N linear subsystems that are described by a state-space model with average-delay is implemented to approximate the dynamics of an IBSS-CLWR. The proposed FNAC contains a neural network consisting of a radial basis function (RBFNN) to learn the uncertainties due to the fuzzy-model error (e.g., the random time-varying delays and the slippage of the CLWR) and the interactions caused by other subsystems. The stability of the overall system is then investigated by adopting the Lyapunov stability theory. Finally, a sequence of experiments including the control of the off-ground CLWR (i.e., the CLWR does not make contact with the ground) and the navigation of the IBSS-CLWR as compared with the conventional proportional-integral-derivative (PID) control is performed to demonstrate the advantage of the proposed control system.**

***Index Terms*—Car-like wheeled robot (CLWR), fuzzy modeling, Internet-based smart space (IBSS) navigation, obstacle avoidance, path tracking, radial basis function neural network, variable structure control.**

I. Introduction

RECENTLY, distributed control applications within sensor networks have been attaining a role of importance (e.g., [1]–[3]). A sensor network that combines both a wireless local area network (WLAN) and Internet network (IN) is called an Internet-based smart space (IBSS) network. It is able to monitor what is occurring within the remote equipment, build its own models, communicate with its inhabitants, and act on the decisions that they make. If the IN and WLAN are absent from IBSS, it is then called smart space (SS). Many problems encountered in classic wheeled robots (e.g., asking for localization [4], requiring high computational power [5], searching for different software for different kinds of mobile robots [6], [7], minimizing the interference with each sensor [8]) are solved when they are in an SS. Due to the constraint of system architecture, a car-like wheeled robot (CLWR) is designed to track a trajectory that is made up of a set of line segments. This paper reveals that using a set of line segments is practical for the path planning.

Based on the concept of IBSS or SS (e.g., [1]–[3]), two distributed charge-coupled device (CCD) cameras are set up in this space to reveal the dynamic positions of both the CLWR and the obstacle. If the system monitoring region is wide, then we need to either increase the number of CCD cameras or consider implementing active CCD cameras. After the images are processed by a server computer, the poses of the CLWR and/or the obstacle together with the outputs of two motors, i.e., steering angle and angular velocity, in the CLWR are transmitted through to the client computer so that a reference input for fuzzy-neural adaptive control (FNAC) is entered. After the control input is transmitted through the system, its results are passed through the Internet to the server computer. It finally reaches the CLWR via a WLAN.

In this paper, the dynamics of an IBSS-CLWR is approximated by the weighted combination of *nine* subsystems described by a linear state equation with nominal input delay. Due to the random time-varying delay characteristic [9], [10], the dynamics of the IBSS-CLWR is first investigated without considering the delay (i.e., the CLWR). That is, the step responses of the CLWR from these nine subsystems in the absence of delay are observed. These nine specific conditions for the step responses are also assigned as the premise variables of the fuzzy rules. This paper is the first to generate a fuzzy model of the CLWR from step responses with various operating conditions. Meanwhile, the delays caused by the signals passing through the IN and WLAN, the time spent in image processing, and the computation time of the control signal, are estimated. As a result, a local linearization of an IBSS-CLWR with respect to nine operating points is described by nine subsystems, which are expressed by a linear state equation with a nominal delay input signal [11]–[14].

A linear transformation (see, e.g., [15]–[17]) is then applied to this time-delay subsystem to obtain a delay-free subsystem. This technique is similar to the "Smith predictor" (e.g., [18] and [19]). In order to shape the response of the closed-loop system, we construct a set of reference models to avoid possible

Manuscript received October 13, 2006; revised March 3, 2007, June 16, 2007, and September 18, 2007; accepted October 15, 2007. First published April 30, 2008; current version published October 8, 2008. This work was supported by the National Science Council of Taiwan, R.O.C., under Grant NSC95-2221-E-032-071.

C.-L. Hwang is with the Department of Electrical Engineering, Tamkang University, Tamsui, Taipei Hsien 25137, Taiwan, R.O.C.

L.-J. Chang is with Marktech International Corporation, Taipei 104, Taiwan, R.O.C.

Color versions of one or more of the figures in this paper are available online at http://ieeexplore.org.

Digital Object Identifier 10.1109/TFUZZ.2008.924319

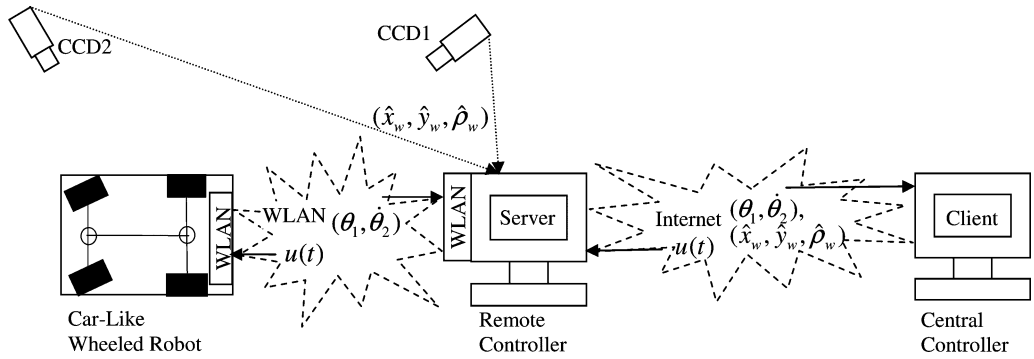

Fig. 1. Block diagram of the overall system.

transient or sluggish response. Based on the delay-free subsystem and its associated reference model (as described earlier), an FNAC is designed. The FNAC is briefly introduced as follows. It contains two parts: one is an equivalent control, and the other is a switching control. As the norm of the sliding surface is inside of a defined set, e.g., $\|\sigma(t)\| < n_{\sigma 2}$, where $\sigma(t)$ denotes a sliding surface which is a linear combination of tracking errors and $n_{\sigma 2}$ is a known constant, a neural network with radial basis function (RBFNN) [20] is employed to learn the uncertainties caused by the fuzzy-model error (e.g., random time-varying delays and the slippage of the CLWR) and the interactions resulting from other subsystems. Upon learning the uncertainties, we design an extra compensation for the equivalent control to enhance system performance. The updating law in the control strategy includes a suitable learning rate and an *e*-modification rate so as to effectively learn the uncertainties without causing the drift of learning weight [21]. It is stressed that the current control is quite different from most of existing papers (e.g., [19] and [22]) in that others try to estimate the uncertainty from the whole nonlinear functions, which in turn causes the learning error to become large and the robust stability and performance of the system to deteriorate. As the norm of the sliding surface is greater than an assigned value, e.g., $\|\sigma(t)\| > n_{\sigma 1} > n_{\sigma 2}$, the updating law will shut down the learning process to avoid the unnecessary transient response and thus prevent instability. To smooth the possibility of discontinuity in the control input, a transition, i.e., $n_{\sigma 1} \geq \|\sigma(t)\| \geq n_{\sigma 2}$, is also considered. Finally, a switching control of the FNAC is executed to cope with the remaining uncertainties, which are not learned by an RBFNN and not tackled by the equivalent control.

No assumption is required for the upper bound of the random time-varying delay of an IBSS-CLWR. However, the uncertainties caused by the fuzzy-model error and the interactions among various subsystems must be relatively bounded. In addition, the stabilizing conditions for every transformed delay-free subsystem must be satisfied. Compared with the approach in this paper, the aforementioned approaches (e.g., [11]) only use a linear control with feedback from the current state. Their robustness is often worse than that using a nonlinear control with feedback from current and past states (e.g., see [15], [17], and [19]). The stability of the overall system is verified by utilizing Lyapunov stability theory. Finally, a sequence of experiments in an IBSS is executed to compare the performances obtained from the FNAC and proportional-integral-derivative (PID) control so as to depict the effectiveness of the control system.

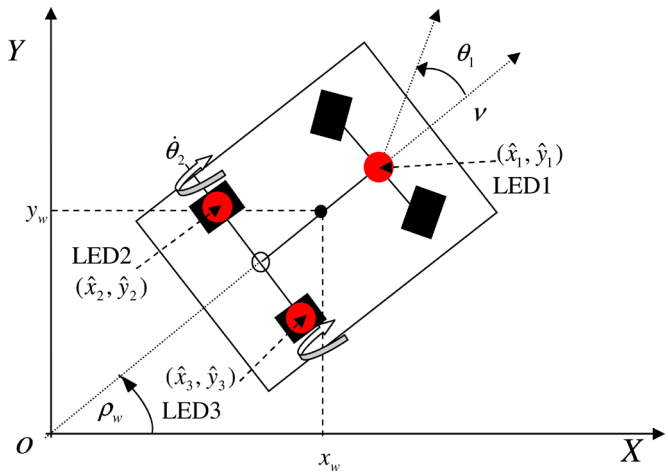

Fig. 2. Kinematics and three positions of the LED for the CLWR.

II. System Description and Problem Formulation

Fig. 1 shows the experimental setup of a CLWR in an IBSS, where $(\hat{x}_w, \hat{y}_w, \hat{\rho}_w)$ denotes the estimated pose of the CLWR, θ_1 is the steering angle of the front-wheel, $\dot{\theta}_2$ is the angular velocity of the rear-wheel, and u is the control input coming from the proposed FNAC or PID control. The overall control system includes a CLWR, two CCD cameras, and two personal computers connected through the Internet. These two personal computers are the sever computer, including the image processing card of Matrox Meteor-II and one WLAN device, and the client computer, executing the path planning and the computation of the FNAC or PID control. The CLWR contains two dc motors from Maxon Corporation, a digital signal processor (DSP) of TMS320LF2407 from TI Corporation, a driver of L298, an 802.11b WLAN device, and a mechanism. For a CLWR with size and shape, its location in the 2-D Cartesian space can be uniquely specified by the spatial position (x_w, y_w) of the base point and the orientation angle ρ_w with respect to the base point (see Fig. 2 or [3]). The WLAN device is used for the data acquisition and transmission between the PC and the CLWR. Three light emitting diodes (LEDs) are set up at

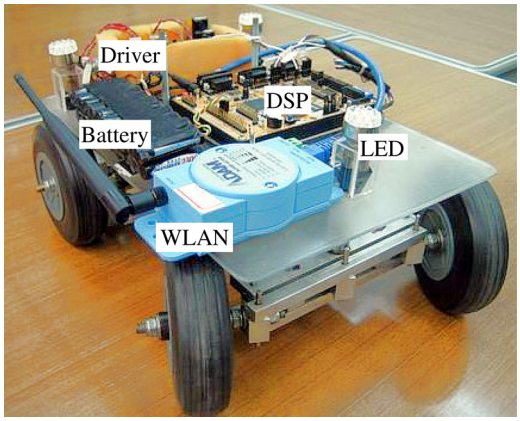

Fig. 3. Realization of the CLWR.

suitable locations; then, three corresponding points on the image plane to represent three positions with respect to the World coordinate, i.e., $(\hat{x}_1, \hat{y}_1), (\hat{x}_2, \hat{y}_2)$, and $(\hat{x}_3, \hat{y}_3)$, as in Fig. 2, are obtained. Finally, the estimated position $\hat{x}_w(k), \hat{y}_w(k)$ and orientation $\hat{\rho}_w(k)$ of the geometry center of the CLWR with respect to the World coordinate at the kth sampling interval is described as follows:

$$\hat{\rho}_w(k) = \tan^{-1}\{[\hat{y}_1(k) - (\hat{y}_2(k) + \hat{y}_3(k))/2] / [\hat{x}_1(k) - (\hat{x}_2(k) + \hat{x}_3(k))/2]\} \quad (1)$$

$$[\hat{x}_w(k), \hat{y}_w(k)] = [(2\hat{x}_1(k) + \hat{x}_2(k) + \hat{x}_3(k))/4, (2\hat{y}_1(k) + \hat{y}_2(k) + \hat{y}_3(k))/4]. \quad (2)$$

Fig. 3 shows the photograph of our CLWR. Upon considering the restriction of selecting a frequency for a CCD (or image processing), the total times needed in the transmission delay in the IN and WLAN, and the total computation times needed for the control algorithm, the sampling time is set at 260 ms. More details are discussed in Section III-B. The maximum estimation error of this CLWR problem is about 2 cm, which is acceptable and only occurs in the periphery of the visible area. Finally, a sequence of experiments, including the control of the off-ground CLWR and the navigation of the IBSS-CLWR, is executed. Comparisons are made between the proposed control and the PID control in order to verify the effectiveness of the current control system.

III. Fuzzy Modeling

Two models are discussed in the fuzzy modeling. The first model does not consider the total times in the transmission delay in the IN and WLAN, and the total computation time of the control algorithm. The second model, to be discussed in Section III-B, incorporates the estimated nominal delays for the transmission in the client computer.

A. Model Without Delay

Before modeling the CLWR, a proportional feedback gain $k_p^1 = 45$ volt/rad for the front-wheel and a forward gain $k_p^2 = 80$ for the rear-wheel are applied to improve the system dynamics so as to obtain a unit dc gain of the rear-wheel (see Fig. 4). They are called enhanced steering and translating subsystems (or ECLWR1 and ECLWR2). In this proposed control system, the output of the front-wheel is the angular position (in radians) and the output of the rear-wheel is the angular velocity (in radians per second). Because the *ranges* of the operations of the front-wheel and rear-wheel are known, and because the *symmetric feature* of the CLWR exists, *nine* operating points as $y_1(t) = x_1(t) = 0°, \pm 15°, \pm 30°$ and $y_2(t) = x_2(t) = 0,\ 20.4,\ \pm 37$ (cm/s) are chosen. Due to the jiggling velocity of the rear-wheel caused by the uncertainties, e.g., loading effect, slippage of the CLWR, an average statistic dynamics is employed to approximate the corresponding dynamics. Hence, each connected system and its associated coupling systems, i.e., all elements of 2×2 transfer function matrix, are supposed to be a 2nd-order system. Based on the resulting step response of a standard 2nd-order system, the corresponding overshoot (M_p) and settling time (T_s) are expressed as follows:

$$M_p = e^{-\pi\xi/\sqrt{1-\xi^2}}, T_s = 4/(\xi w_n)(2\% \text{ criterion}) \quad (3)$$

where ξ and ω_n denote, respectively, the damping ratio and natural frequency of the transfer function $G(s) = \omega_n^2/(s^2 + 2\xi\omega_n s + \omega_n^2)$. Therefore, two equations can be formed to associate with these two unknowns ξ and ω_n. The dynamics of the ith operating condition of the CLWR is expressed by the following two-input–two-output transfer function matrix:

$$Y^i(s) = G^i(s)U^i(s) \quad (4)$$

where $Y^i(s),\ U^i(s) \in \Re(s)^{2\times 1}$, and $G^i(s) = \in \Re(s)^{2\times 2}$. Define $G^i_{jk}(s)$ as the transfer function of the jth row and the kth column for $G^i(s)$, or the relation between the kth input and the jth output of the ith subsystem. Because the angular velocity of the rear-wheel does not have influence on the output of the front-wheel, it has the result $G^i_{12}(s) = 0$; i.e., the system output 1 (i.e., $y_1(t)$) is not affected by the system input 2 [i.e., $u_2(t)$].

Remark 1: There are *two connected systems* for the model of the CLWR or IBSS-CLWR. However, in the fuzzy modeling of the CLWR or IBSS-CLWR, it contains *nine subsystems.* Each subsystem corresponds to one operating condition. These modeling representations are different.

Subsystem 1 is defined as the system corresponding to the operating point or step input $U^1(s) = [30/s \quad 37/s]^T$ with the unit degree and centimeter per second, respectively. The resulting step responses are shown in Fig. 5(a) and (b). The first subsystem is then approximated by the following transfer function matrix from these resulting step responses:

$$G^1_{11}(s) = 250.457/(s^2 + 22.857s + 250.457)$$
$$G^1_{22}(s) = 19.377/(s^2 + 7.273s + 19.377)$$
$$G^1_{21}(s) = -0.18/(s^2 + 7.273s + 19.377). \quad (5)$$

Based on other eight step inputs and their associated step responses, as listed in Table I, we have the following transfer functions for the other eight subsystems.

$$G^2_{11}(s) = G^1_{11}(s), G^2_{22}(s) = 32.915/(s^2 + 8s + 32.915)$$
$$G^2_{21}(s) = -0.315/(s^2 + 8s + 32.915)$$

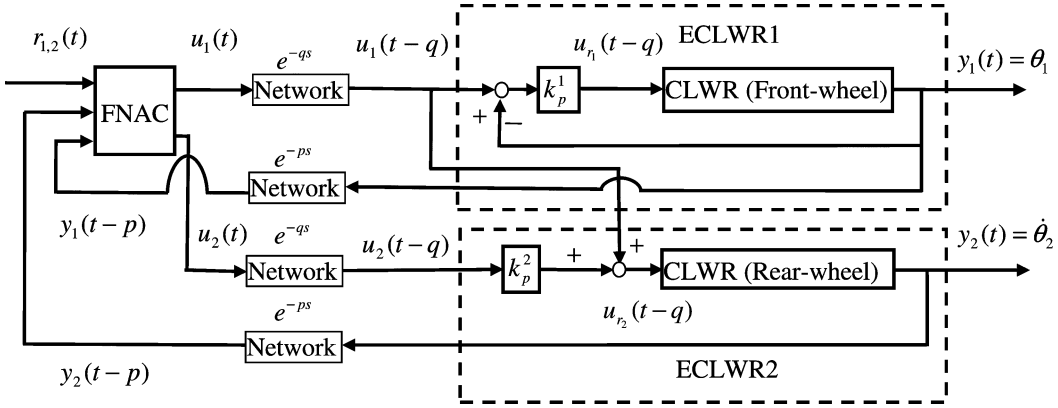

Fig. 4. Enhanced CLWR by two proportional (feedback and forward) gains.

$$
\begin{aligned}
&G_{11}^3(s)=G_{11}^1(s), G_{22}^3(s)=G_{22}^2(s), G_{21}^3(s)=0\\
&G_{11}^4(s)=557.546/(s^2+30.189s+557.546)\\
&G_{22}^4(s)=G_{22}^1(s)\\
&G_{21}^4(s)=-0.12/(s^2+7.273s+19.377)\\
&G_{11}^5(s)=G_{11}^4(s), G_{22}^5(s)=G_{22}^2(s)\\
&G_{21}^5(s)=-0.25/(s^2+8s+32.915)\\
&G_{11}^6(s)=G_{11}^4(s), G_{22}^6(s)=G_{22}^3(s), G_{21}^6(s)=0\\
&G_{11}^7(s)=G_{11}^4(s), G_{22}^7(s)=G_{22}^1(s), G_{21}^7(s)=0\\
&G_{11}^8(s)=G_{11}^4(s), G_{22}^8(s)=G_{22}^2(s), G_{21}^8(s)=0\\
&G_{11}^9(s)=G_{11}^4(s), G_{22}^9(s)=G_{22}^3(s), G_{21}^9(s)=0. \qquad (6)
\end{aligned}
$$

Because the state space approach is used in the controller design of the FNAC, the following state-space equations are formed to represent the transfer functions of (5) and (6):

$$\dot{x}(t)=A^i x(t)+B^i u(t),\ y(t)=C^i x(t), \quad i=1,2,\ldots,9 \qquad (7)$$

where

$$A^i=\begin{bmatrix} 0 & 0 & 1 & 0\\ 0 & 0 & 0 & 1\\ a_{31}^i & a_{32}^i & a_{33}^i & a_{34}^i\\ a_{41}^i & a_{42}^i & a_{43}^i & a_{44}^i \end{bmatrix}, \quad B^i=\begin{bmatrix} 0 & 0\\ 0 & 0\\ b_{31}^i & b_{32}^i\\ b_{41}^i & b_{42}^i \end{bmatrix}$$

$$C^i=\begin{bmatrix} 1 & 0 & 0 & 0\\ 0 & 1 & 0 & 0 \end{bmatrix}. \qquad (8)$$

The corresponding transfer function matrix possesses the following transfer function entries:

$$
\begin{aligned}
G_{11}^i(s)&=b_{31}^i/\left(s^2-a_{33}^i s-a_{31}^i\right)\\
G_{12}^i(s)&=\left[b_{32}^i s^2+\left(a_{44}^i b_{32}^i-a_{34}^i b_{42}^i\right)s+\left(a_{42}^i b_{32}^i-a_{32}^i b_{42}^i\right)\right]\\
&\quad /\left[\left(s^2-a_{33}^i s-a_{31}^i\right)\left(s^2-a_{44}^i s-a_{42}^i\right)\right]\\
G_{21}^i(s)&=\left[b_{41}^i s^2+\left(a_{43}^i b_{31}^i-a_{33}^i b_{41}^i\right)s+\left(a_{41}^i b_{31}^i-a_{31}^i b_{41}^i\right)\right]\\
&\quad /\left[\left(s^2-a_{33}^i s-a_{31}^i\right)\left(s^2-a_{44}^i s-a_{42}^i\right)\right]\\
G_{22}^i(s)&=b_{42}^i/\left(s^2-a_{44}^i s-a_{42}^i\right). \qquad (9)
\end{aligned}
$$

By comparing (5) and (6) with (9), we have

$$
\begin{aligned}
&b_{32}^i s^2+\left(a_{44}^i b_{32}^i-a_{34}^i b_{42}^i\right)s+\left(a_{42}^i b_{32}^i-a_{32}^i b_{42}^i\right)=0,\\
&b_{41}^i\left[s^2+\left(a_{43}^i b_{31}^i-a_{33}^i b_{41}^i\right)s/b_{41}^i+\left(a_{41}^i b_{31}^i-a_{31}^i b_{41}^i\right)/b_{41}^i\right]\\
&=k\left(s^2-a_{33}^i s-a_{31}^i\right) \qquad (10)
\end{aligned}
$$

where k is a suitable constant. Then, the solution of (10) is

$$a_{32}^i=a_{34}^i=a_{41}^i=a_{43}^i=b_{32}^i=0, \text{ and } k=b_{41}^i. \qquad (11)$$

Finally, the coefficients of these *nine* subsystems, as in (7) and (8), are given as

$$
\begin{aligned}
a_{31}^{1\sim 9}&=-250.457,-250.457,-250.457,-557.546\\
&\quad -557.546,-557.546,-557.546,-557.546,-557.546\\
a_{33}^{1\sim 9}&=-22.857,-22.857,-22.857,-30.189\\
&\quad -30.189,-30.189,-30.189,-30.189,-30.189\\
a_{42}^{1\sim 9}&=19.377,-32.915,-32.915,-19.377\\
&\quad -32.915,-32.915,-19.377,-32.915,-32.915\\
a_{44}^{1\sim 9}&=-7.273,-8,-8,-7.273,-8,-8,-7.273,-8,-8\\
b_{31}^{1\sim 9}&=250.457,250.457,250.457,\ 557.546\\
&\quad 557.546,557.546,557.546,557.546,557.546\\
b_{41}^{1\sim 9}&=-0.18,-0.315,0,-0.18,-0.375,0,0,0,0\\
b_{42}^{1\sim 9}&=19.377,32.915,32.915,19.377,\\
&\quad 32.915,32.915,19.377,32.915,32.915\\
a_{32}^{1\sim 9}&=a_{34}^{1\sim 9}=a_{41}^{1\sim 9}=a_{43}^{1\sim 9}=b_{32}^{1\sim 9}=0. \qquad (12)
\end{aligned}
$$

B. Model With Nominal Delay

From Fig. 1, the total delay is estimated as 160 ms, which includes the transmission delay from the client computer through the WLAN to the server computer, the image processing time in the server computer, and the time through the Internet between the server computer and client computer. Similarly, by using the reverse path from the server computer to the client computer without image processing time, its delay time is estimated to be 100 ms. Based on these two estimations, the total computation

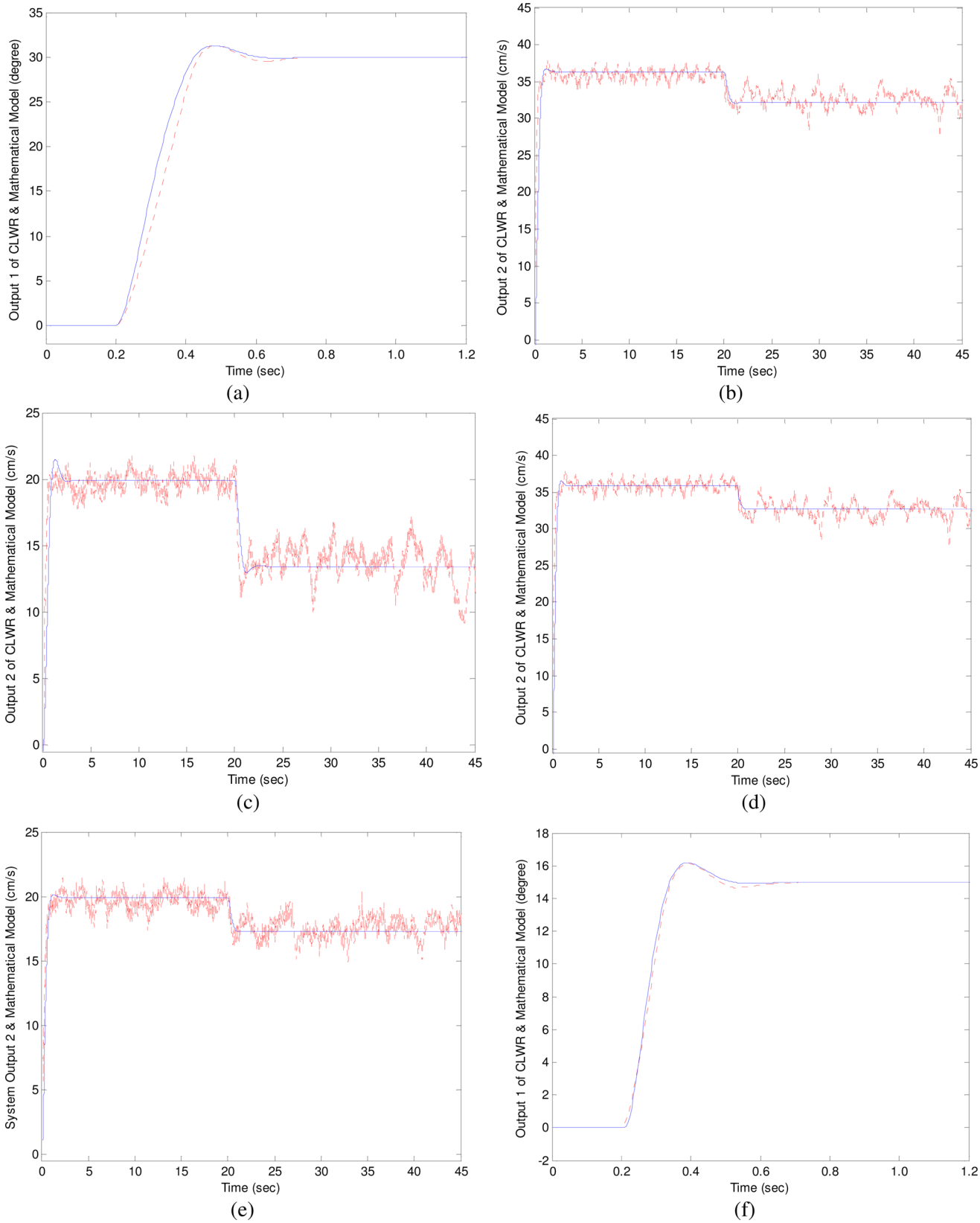

Fig. 5. Step responses of the mathematical models and the CLWR for various conditions. (a) The front-wheel for $v_d = 37$ cm/s at $t = 0$ s and $\theta_{1d} = 30^\circ$ at $t = 0.2$ s$(\cdots)$; the $G_{11}^{1\sim3}(s)$ $(-)$. (b) The rear-wheel for $v_d = 37$ cm/s at $t = 0$ s and $\theta_{1d} = 30^\circ$ at $t = 20$ s$(\cdots)$; the $G_{21}^{1}(s), G_{22}^{1,4,7}(s)$ $(-)$. (c) The rear-wheel for $v_d = 20.4$ cm/s at $t = 0$ s and $\theta_{1d} = 30^\circ$ at $t = 20$ s$(\cdots)$; the $G_{21}^{2}(s), G_{22}^{2,3,5,8}(s)(-)$. (d) The rear-wheel for $v_d = 37$ cm/s at $t = 0$ s and $\theta_{1d} = 15^\circ$ at $t = 20$ s$(\cdots)$; the $G_{21}^{4}(s), G_{22}^{1,4,7}(s)$ $(-)$. (e) The rear-wheel for $v_d = 20.4$ cm/s at $t = 0$ s and $\theta_{1d} = 15^\circ$ at $t = 20$ s$(\cdots)$; the $G_{21}^{5\sim6}(s), G_{22}^{2,3,5,8}(s)(-)$. (f) The front-wheel for $v_d = 37$ cm/s at $t = 0$ s and $\theta_{1d} = 15^\circ$ at $t = 0.2$ s$(\cdots)$; the $G_{11}^{4\sim9}(s)$ $(-)$.

TABLE I
STEP INPUTS AND THEIR CORRESPONDING STEP RESPONSES OF NINE SUBSYSTEMS

Subsystem i	1	2	3	4	5	6	7	8	9
Step Input $U^i(s)$	$\begin{bmatrix} 30/s \\ 37/s \end{bmatrix}$	$\begin{bmatrix} 30/s \\ 20.4/s \end{bmatrix}$	$\begin{bmatrix} 30/s \\ 0 \end{bmatrix}$	$\begin{bmatrix} 15/s \\ 37/s \end{bmatrix}$	$\begin{bmatrix} 15/s \\ 20.4/s \end{bmatrix}$	$\begin{bmatrix} 15/s \\ 0 \end{bmatrix}$	$\begin{bmatrix} 0 \\ 37/s \end{bmatrix}$	$\begin{bmatrix} 0 \\ 20.4/s \end{bmatrix}$	$\begin{bmatrix} 0 \\ 0 \end{bmatrix}$
Step Response	Figs. 5(a),(b)	Figs. 5(c),(d)	Fig. 5(b)	Figs. 5(d),(f)	Figs. 5(e),(f)	Fig. 5(f),	Fig. 5(a)	Fig. 5(c)	-

time of the proposed control is smaller than the total delay time of the signal transmission and the time required for the image processing. Therefore, the transfer function matrix of the ith subsystem becomes

$$Y^i(s) = G^i(s)U^i(s)\, e^{-(p+q)s} \tag{13}$$

where $p = 0.16$ s and $q = 0.1$ s denote, respectively, the input and output delays of the client computer. The corresponding state and output equations for the ith subsystem (13) are described as follows:

$$\dot{x}(t) = A^i x(t) + B^i u(t-\tau),\ y(t) = C^i x(t), \quad i = 1, 2, \ldots, 9 \tag{14}$$

where $\tau = p + q = 0.26$ s, $A^i \in \Re^{4\times 4}$, $B^i \in \Re^{4\times 2}$, and $C^i \in \Re^{2\times 4}$ have the same form as (8). In summary, the ith rule of the fuzzy model for the IBSS-CLWR is

System rule i: IF $y_1(t)$ is M_1^i, and $y_2(t)$ is M_2^i

$$\text{THEN } \dot{x}(t) = A^i x(t) + B^i u(t-\tau) \tag{15a}$$

where $[y_1(t)y_2(t)]^T = y(t) = [x_1(t)x_2(t)]^T$, and $M_j^i, j = 1, 2$, $i = 1, 2, \ldots, 9$ denote fuzzy terms of M_j selected for *rule i* that have the following form:

$$M_1^{1\sim 3}(y_1) = \begin{cases} e^{-(y_1(t)\pm 30^\circ)^{2/50}}, & \text{if } |y_1(t)| \geq 30^\circ \\ 1, & \text{otherwise} \end{cases},$$

$$M_1^{4\sim 6}(y_1) = e^{-(y_1(t)\pm 15^\circ)^{2/50}}, M_1^{7\sim 9}(y_1) = e^{-y_1^2(t)/50} \tag{15b}$$

$$M_2^{1,4,7}(y_2) = \begin{cases} e^{-(y_2(t)\pm 37)^{2/60}}, & \text{if } |y_2(t)| \geq 37 \text{ cm/s} \\ 1, & \text{otherwise} \end{cases},$$

$$M_2^{2,5,8}(y_2) = e^{-(y_2(t)\pm 20.4)/60}, M_2^{3,6,9}(y_2) = e^{-y_2^2(t)/50}. \tag{15c}$$

Furthermore, the stable reference models for every subsystem are assumed to be

$$C_0^i = \begin{bmatrix} 0 & 0 & 1 & 0 \\ 0 & 0 & 0 & 1 \\ c_{031}^i & 0 & c_{033}^i & 0 \\ 0 & c_{042}^i & 0 & c_{044}^i \end{bmatrix}, D_0^i = \begin{bmatrix} 0 & 0 \\ 0 & 0 \\ d_{031}^i & 0 \\ 0 & d_{042}^i \end{bmatrix} \tag{16}$$

where $c_{031}^i = -100, c_{033}^i = -40, c_{042}^i = -10, c_{044}^i = -20$, $d_{031}^i = 100$, and $d_{042}^i = 10$.

IV. CONTROLLER DESIGN

Fig. 6 contains three subsections to describe the proposed controller design. Three theorems are also derived to discuss the properties of the proposed FNAC.

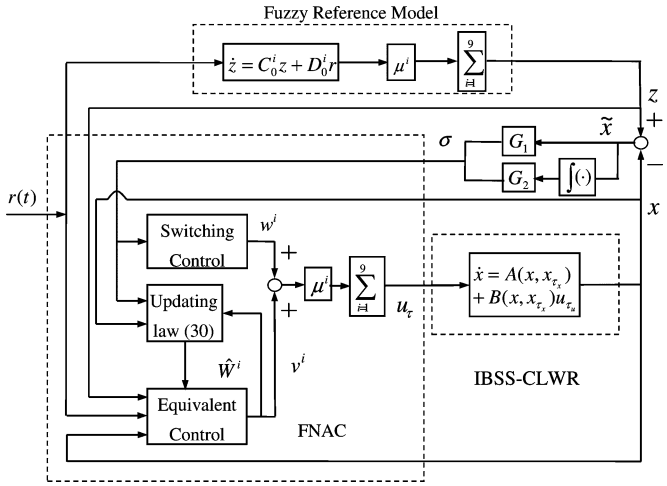

Fig. 6. Control block diagram of the proposed control system.

A. Background of Controller Design

The dynamics of an IBSS-CLWR is assumed to be

$$\dot{x}(t) = A(x, x_{\tau_x}) + B(x, x_{\tau_x})u_{\tau_u}(t) \tag{17}$$

where $x(t) \in \Re^4$ denotes the available system state, $x_{\tau_x}(t) = x(t - \tau_x(t))$ the time-varying delayed state, and $u_{\tau_u}(t) = u(t - \tau_u(t)) \in \Re^2$ the time-varying delayed input. In addition, $\tau_x(t) \geq 0$ and $\tau_u(t) \geq 0$ denote random quantities of the time-varying delays of the state and the input, respectively; with the expected values fixed and known, i.e., $E\{\tau_x(t)\} = p$, $E\{\tau_u(t)\} = q$. The continuous mappings: $A(x, x_{\tau_x}) : \Re^8 \to \Re^4$, and $B(x, x_{\tau_x}) : \Re^8 \to \Re^{4\times 2}$ are partially known. The initial condition of the system (17) is assumed to be bounded and known, i.e., $x(\varsigma_x) = x_0(\varsigma_x) \in \Re^4$ and $u(\varsigma_u) = u_0(\varsigma_u) \in \Re^2$, where $\varsigma_x \in [-\tau_x(t), 0], \varsigma_u \in [-\tau_u(t), 0]$. In summary, the dynamics of (17) is approximated by the weighted combinations of nine subsystems (15):

$$\dot{x}(t) = \sum\nolimits_{i=1}^{9} \mu^i(x)[A^i x(t) + B^i u_\tau(t)] \tag{18}$$

where $\mu^i(x) = k^i(x)/\sum_{i=1}^{9} k^i(x)$, $k^i(x) = M_1^i(x_1)M_2^i(x_2)$ and $u_\tau(t) = u(t-\tau)$. In addition, $\mu^i(x) \geq 0 \forall i$ and $\sum_{i=1}^{9} \mu^i(x) = 1$. The following linear transformation (19) (see, e.g., [15]–[17]) is applied to the time delayed subsystem (15) such that a delay-free subsystem (20) is obtained

$$\bar{x}(t) = x(t) + \int_{-\tau}^{0} e^{A^i \vartheta} B^i u_{\tau+\vartheta}(t) d\vartheta \tag{19}$$

where $\bar{x} \in \Re^4$ and the integration of $\vartheta \in [-\tau, 0]$ for the input delay. After the linear transformation, the fuzzy system rule (15) is rewritten as follows:

System rule i: IF x_1 is M_1^i and x_2 is M_2^i

$$\text{THEN } \dot{\bar{x}}(t) = A^i \bar{x}(t) + \bar{B}^i u(t), \quad \text{for} \quad i = 1, 2, \ldots, 9 \tag{20}$$

where $\bar{B}^i = e^{-\tau A_j^i} B^i$. The pair $(A^i, \bar{B}^i)$, for $i = 1, 2, \ldots, 9$ must be stabilizable (or controllable). The output of the overall fuzzy system is then described as

$$\dot{\bar{x}}(t) = \sum_{i=1}^{9} \mu^i(x)[A^i \bar{x}(t) + \bar{B}^i u(t)] \tag{21}$$

where $\mu^i(x), i = 1, 2, \ldots, 9$ is the same as (18). Based on the approximation of the Takagi–Sugeno model [11], [12], the following uncertain matrices $\Delta A(x, x_{\tau_x}, t)$ and $\Delta B(x, x_{\tau_x}, t) u_{\tau_u}(t)$ exist. These are denoted as the approximation error in the fuzzy modeling, derived from (17), (19), (21), and Leibnitz' rule, and are described as follows:

$$\Delta B(x, x_{\tau_x}, t) u_{\tau_u}(t) = -\int_{-\tau}^{0} e^{\bar{A}^i \theta} B^i \dot{u}_{\tau+\theta}(t) d\theta \tag{22}$$

$$A_n(x) + B_n(x) u_\tau(t) = \sum_{i=1}^{9} \mu^i(x)[A^i \bar{x}(t) + \bar{B}^i u(t)] \tag{23}$$

where $\dot{u}_{\tau+\theta}(t) = du_{\tau+\theta}(t)/dt$, $A(x, x_{\tau_x}) = A_n(x) + \Delta A(x, x_{\tau_x}, t)$ and $B(x, x_{\tau_x}) u_{\tau_u}(t) = B_n(x) u(t) + \Delta B(x, x_{\tau_x}, t) u_{\tau_u}(t)$. Assuming the reference model shares the same fuzzy sets with the fuzzy subsystem (15), we have the following rule for the reference model:

Reference Model Rule i: IF x_1 is M_1^i and x_2 is M_2^i

$$\text{THEN } \dot{z}(t) = C_0^i z(t) + D_0^i r(t) \tag{24}$$

where $C_0^i \in \Re^{4\times 4}$, $\Re\mathrm{e}\{\lambda[C_0^i]\} < 0$, $D_0^i \in \Re^{4\times 2}$, for $i = 1, 2, \ldots, 9$, and $r(t) \in \Re^2$ is a known reference input. The output of the overall fuzzy reference model system is

$$\dot{z}(t) = \sum_{i=1}^{9} \mu^i(x)\left[C_0^i z(t) + D_0^i r(t)\right]. \tag{25}$$

Remark 2: The coefficients of the reference model of the ith subsystem, i.e., C_0^i and D_0^i for $i = 1, 2, \ldots, 9$, are selected such that the transfer function matrices $G_m^i(s) = C_m^i[sI_n - C_0^i]^{-1} D_0^i + D_m^i$ are stable, with desired poles and zeros, and with unity dc gain (by suitable selected matrices C_m^i and D_m^i).

Before discussing the controller design, the following sliding surface is defined

$$\sigma(t) = G_1 \tilde{x}(t) + G_2 \int \tilde{x}(\tau)\, d\tau \tag{26}$$

where $\tilde{x}(t) = x(t) - z(t)$ denotes the tracking error and G_1 and $G_2 \in \Re^{2\times 4}$ are chosen such that the dynamics of $\sigma(t) = 0$ is Hurwitz. In the selection of G_1 and G_2, it can also adjust the frequency response between the tracking error and the sliding surface. Based on the concept of parallel distribution control (PDC), (e.g., [11] and [12]), the proposed FNAC is supposed to share the same fuzzy sets with the subsystem (15).

Controller Rule i: IF x_1 is M_1^i and x_2 is M_2^i

$$\text{THEN } u(t) = v^i(t) + w^i(t). \tag{27}$$

The aforementioned FNAC of subsystem i contains an equivalent control (28a), i.e., $v^i(t)$, to deal with a nominal system including the learning uncertainties, and a switching control (28b), i.e., $w^i(t)$, to cope with the remaining uncertainties, which are not effectively learned by an RBFNN and not tackled by the equivalent control

$$\begin{aligned} v^i(t) = & -(G_1 \bar{B}^i)^{-1}\{G_1 A^i \bar{x}(t) - G_1 D_0^i r(t) - G_1 C_0^i z(t) \\ & + G_2 \tilde{x}(t) + F(\|\sigma(t)\|)\hat{W}^i(t)^T \Phi(\rho)\} \end{aligned} \tag{28a}$$

$$\begin{aligned} w^i(t) = & -(G_1 \bar{B}^i)^{-1}\left\{\eta_1^i \sigma(t) + \eta_2^i \sigma(t)/[\|\sigma(t)\| + \varepsilon^i]\right\} \\ & /(\sqrt{2} - \alpha^i) \end{aligned} \tag{28b}$$

where $G_1 \bar{B}^i$ is nonsingular, $\eta_1^i = \mathrm{diag}\{\eta_{11}^i,\ \eta_{12}^i\} > 0$ and $\eta_2^i = \mathrm{diag}\{\eta_{21}^i,\ \eta_{22}^i\} > 0$ are the switching gains, $\varepsilon^i > 0$, the symbol $\|\sigma(t)\|$ represents an Euclidean norm of the vector $\sigma(t)$, and α^i satisfies the following inequality:

$$\begin{aligned} & \|G_1 \Delta B(x, x_{\tau_x}, t)(G_1 \bar{B}^i)^{-1}\|_F \le \alpha^i \le \sqrt{m} \\ & \qquad \forall i, x(t), x_{\tau_x}(t), t \end{aligned} \tag{28c}$$

where $m = 2$ denotes the number of the control inputs, the notation $\|\cdot\|_F$ denotes the Frobenius norm, i.e., $\|W\|_F^2 = \mathrm{tr}[W^T W] = \mathrm{tr}[W W^T]$, $W \in \Re^{L\times 2}$. In addition, the scalar function in (28a) is designed as

$$F(\|\sigma(t)\|) = \begin{cases} 0, & \text{as } \|\sigma(t)\| > n_{\sigma 1} \\ 1, & \text{as } \|\sigma(t)\| < n_{\sigma 2} \\ (n_{\sigma 1} - \|\sigma(t)\|)/(n_{\sigma 1} - n_{\sigma 2}), & \text{otherwise} \end{cases} \tag{29}$$

where $n_{\sigma 1} > h_{\max} > n_{\sigma 2} > p_{\max} \in \Re^+$ (see Section IV-B and IV-C for the details). The following updating law (30) is employed to obtain the weighting parameter for the equivalent control (28a)

$$\dot{\hat{W}}^i(t) = \beta^i \Phi(\rho)\sigma^T(t) - \gamma^i \hat{W}^i(t) \tag{30a}$$

where $\beta^i \in \Re^+$ denotes a learning rate, $\gamma^i \in \Re^+$ denotes an *e*-modification rate to ensure the boundedness of the learning weight, $\hat{W}^i(t) \in \Re^{L\times 2}$ stands for the learning weight, and $\Phi(\rho) \in \Re^L$ represents the basis function of the RBFNN

$$\Phi(\rho) = [\,1 \quad \phi_2(\rho) \quad \ldots \quad \phi_L(\rho)\,]^T \tag{30b}$$

where $\phi_j(\rho) = \exp[-\|\rho(t) - c_j\|^2/\zeta_j^2]$, L, c_j, ζ_j for $j = 2, 3, \ldots, L$ are known, the centers c_j for $j = 2, 3 \ldots, L$ are chosen with normal distribution in the corresponding domain, and $\rho(t) = [x^T(t) \quad v^i(t)^T]^T$. Because the switching control (28b) is applied to deal with the uncertainties, one cannot use a signal that deals with uncertainties to represent the uncertainties. Hence, $\rho(t)$ cannot contain $w^i(t)$. Finally, the overall control law is described as follows:

$$u(t) = \sum_{i=1}^{9} \mu^i(x)[v^i(t) + w^i(t)]. \tag{31}$$

Remark 3: The motivation for designing the proposed control (31) and how it works are explained in the third paragraph of Section I. Due to space limitation, we do not repeat it here.

The following equation describes the system uncertainties caused by the approximation error in fuzzy modeling and the interactions resulting from other subsystems

$$\Omega^i(\rho)+\varepsilon_\Omega^i(t)=G_1\Big\{\Delta A(x,x_{\tau_x},t)+\bar{B}^i[u(t)-u^i(t)]+\Delta B(x,x_{\tau_x},t)\sum\nolimits_{j=1,j\neq i}^{9}\mu^j(x)w^j(t)+\Delta B(x,x_{\tau_x},t)u_{\tau_u}(t)\Big\} \tag{32}$$

where $\Omega^i(\rho)$ is a function of $\rho(t)$ due to (28), (21), and (32), and $\varepsilon_\Omega^i(t)$ denotes the other uncertainties except $\Omega^i(\rho)$. In general, the magnitude of $\varepsilon_\Omega^i(t)$ is upper bounded by a constant. The right-hand side of (32) is divided into two terms: one is $\Omega^i(\rho)$, which can be estimated by an upper bounded function or approximated by a neural network, and the other is $\varepsilon_\Omega^i(t)$, which cannot be estimated by an upper bounded function or approximated by a neural network.

B. Condition: $\|\sigma(t)\|>n_{\sigma 1}$

The following property about "uniformly ultimately bounded (UUB)" is first defined.

Definition 1: The solution of a dynamic system is said to be UUB if there exist positive constants υ and κ, and for every $\delta\in(0,\kappa)$, there is a positive constant $T=T(\delta)$ such that $\|x(t_0)\|<\delta\Rightarrow\|x(t)\|\leq\upsilon,\forall t\geq t_0+T$.

From (29), $F(\|\sigma(t)\|)=0$ (or $\hat{W}^i(t)=0$) as $\|\sigma(t)\|>n_{\sigma 1}$. Using (17), (20)–(23), (25)–(27), and (31), the derivative of sliding surface is given as follows:

$$\begin{aligned}\dot{\sigma}(t)&=G_1[\dot{x}(t)-\dot{z}(t)]+G_2\tilde{x}(t),\text{ using (26)}\\&=G_1\Big\{A(x,x_{\tau_x})+B(x,x_{\tau_x})u_{\tau_u}(t)-\sum_{i=1}^{9}\mu^i(x)[C_0^iz(t)+D_0^ir(t)]\Big\}\\&\quad+G_2\tilde{x}(t),\text{ using (17) and (25)}\\&=G_1\Big\{\sum_{i=1}^{9}\mu^i(x)[A^i\bar{x}(t)+\bar{B}^iu(t)]+\Delta A(x,x_{\tau_x},t)+\Delta B(x,x_{\tau_x},t)u_{\tau_u}(t)\Big\}\\&\quad-G_1\Big\{\sum_{i=1}^{9}\mu^i(x)\big[C_0^iz(t)+D_0^ir(t)\big]\Big\}\\&\quad+G_2\tilde{x}(t),\text{ using (21)–(23)}\\&=\sum_{i=1}^{9}\mu^i(x)G_1\times\Big\{A^i\bar{x}(t)+\Delta A(x,x_{\tau_x},t)+(\bar{B}^i+\Delta B(x,x_{\tau_u},t))\times\sum_{j=1}^{9}\mu^j(x)(v^j(t)+w^j(t))-\big[C_0^iz(t)+D_0^ir(t)\big]\Big\}\\&\quad+G_2\tilde{x}(t),\text{ using (27)},\sum_{i=1}^{9}\mu^i(x)=1\\&=\sum_{i=1}^{9}\mu^i(x)\Big\{G_1A^i\bar{x}(t)+G_1\Delta A(x,x_{\tau_x},t)+G_1\bar{B}^iv^i(t)+G_1\bar{B}^i\sum_{j=1,j\neq i}^{9}\mu^j(x)v^j(t)+G_1\Delta B(x,x_{\tau_x},t)v^i(t)\\&\quad+G_1(\bar{B}^i+\Delta B(x,x_{\tau_x},t))w^i(t)+G_1(\bar{B}^i+\Delta B(x,x_{\tau_x},t))\times\sum_{j=1,j\neq i}^{9}\mu^j(x)w^j(t)-G_1\big[C_0^iz(t)+D_0^ir(t)\big]\Big\}+G_2\tilde{x}(t).\end{aligned} \tag{33}$$

Substituting $v^i(t)$ from (28a) into (33) yields

$$\dot{\sigma}(t)=\sum_{i=1}^{9}\mu^i(x)\big\{[I+G_1\Delta B(x,x_{\tau_x},t)(G_1\bar{B}^i)^{-1}]\cdot(G_1\bar{B}^i)w^i(t)+\Omega^i(\rho)+\varepsilon_\Omega^i(t)\big\} \tag{34}$$

where $\Omega^i(\rho)+\varepsilon_\Omega^i(t)$ is described in (32) and their upper bounds are estimated as follows:

$$\|\Omega^i(\rho)\|\leq h_\Omega^i(\rho),\big\|\varepsilon_\Omega^i(t)\big\|\leq h_\varepsilon^i. \tag{35}$$

Then, the following theorem is given for the operating point outside of $\|\sigma(t)\|=n_{\sigma 1}$.

Theorem 1: Consider the nonlinear time-varying delayed system (17) and the FNAC (28) with $F(\|\sigma(t)\|)=0$ or $\hat{W}^i(t)=0$, $\|\eta_1^i\|_F>\delta/2>0$ and $\|\eta_2^i\|_F>h_\Omega^i+h_\varepsilon^i$. Together with the conditions (28c) and (35), $\sigma(t)$ and $u(t)$ are UUB and the tracking performance is achieved as follows:

$$P_r=\{\sigma(t)\in\Re^2|0\leq\|\sigma(t)\|\leq h_{\max}\} \tag{36}$$

where $h_{\max}=\max\limits_{1\leq i\leq 9}[h^i(\rho)]$, $h^i(\rho)=\sqrt{[h_1^i(\rho)]^2+h_2^i(\rho)}-h_1^i(\rho)$, $h_1^i(\rho)=\{\varepsilon^i+[\|\eta_2^i\|_F-h_\Omega^i(\rho)-h_\varepsilon^i]/(\|\eta_1^i\|_F-\delta/2)\}/2$ and $h_2^i(\rho)=\varepsilon^i(h_\Omega^i(\rho)+h_\varepsilon^i)/(\|\eta_1^i\|_F-\delta/2)$.

Proof: See Appendix A.

Remark 4: If $\varepsilon^i=0$ (i.e., no boundary layer for the ith fuzzy subsystem), then from (36), $h_{\max}=0$. Hence, $\|\sigma(t)\|\to 0$ (or $\|\tilde{x}(t)\|\to 0$) as $t\to\infty$. However, the control input may be in a chattering way and its amplitude is also large if the upper bound of uncertainties is large. Although a large value of ε^i will make the control input smooth, the tracking accuracy is generally degraded. Therefore, a compromise must be made. This is an important design consideration that the system uncertainties must be learned and an extra compensation function designed so that the tracking accuracy and the degree of chattering control input are improved. Furthermore, if the uncertainties do not exist, i.e., $h_\Omega^i(\rho)=0$ and $h_\varepsilon^i=0$, then from (36), $h_{\max}=0$. Hence, $\|\tilde{x}(t)\|\to 0$ as $t\to\infty$.

Remark 5: The assumptions of Theorem 1 are explained as follows:

1) Condition (28c) denotes the uncertainty of the control gain as compared to its nominal value. It indicates that this uncertainty must be smaller than the corresponding nominal value.
2) Condition (35) denotes the must known upper bound of the uncertainty. Its upper bound is interrelated with the system performance. From (36), the larger the $h_\Omega^i(\rho)$ or h_ε^i, the larger the $\|\sigma(t)\|$ (or tracking error).

C. Condition: $\|\sigma(t)\| < n_{\sigma 2}$

When $\|\sigma(t)\| < n_{\sigma 2}$, the updating law (30) is employed to learn the uncertainty $\Omega^i(\rho)$. It is assumed that the unknown signals $\Omega^i(\rho)$ can be smoothly truncated outside of $\rho(t) \in \Psi(\rho)$ (a compact subset in $\Re^{12}$). Hence, their spatial Fourier transformations are absolutely integrable. The following universal approximation theory (e.g., [20]–[22]) is first stated.

Theorem 2: Suppose $\rho(t) \in \Psi(\rho)$ (a compact subset of $\Re^{12}$), $f(\rho) : \Psi \to \Re^2$ is a continuous function vector. For an arbitrary constant $\varepsilon > 0$, there exists an integer L (the number of hidden neurons) and real constant matrix $W \in \Re^{L\times 2}$, where $\|W\|_F^2 \le W_m$, such that

$$f(\rho) = W^T \Phi(\rho) + \varepsilon_f(\rho)$$

where $\|\varepsilon_f(\rho)\| \le \varepsilon \quad \forall \rho(t) \in \Psi(\rho)$.

Based on the result of Theorem 2, the system uncertainties in a compact subset $\Psi(\rho)$ are assumed to be continuous and approximated by the following RBFNN:

$$\Omega^i(\rho) = (W^i)^T \Phi(\rho) + \upsilon^i(\rho) \tag{37}$$

where $W^i \in \Re^{L\times 2}$ is a constant matrix that is not necessarily unique, $\|\upsilon^i(\rho)\| \le p_\upsilon^i \forall \rho(t) \in \Psi(\rho)$, where $p_\upsilon^i \ll h_\Omega^i(\rho)$. In fact, $\upsilon^i(\rho)$ for $i = 1, 2, \ldots, 9$ are regarded as the summation of the class membership error, the aliasing error, and the truncation error [22]. In addition, the upper bound of W^i is known, i.e., $\|W^i\|_F \le W_m^i$. The compact subsets $\Psi(\rho)$ can be achieved because the result of *Theorem 1* ensures the boundedness of $\upsilon(t)$. Similarly, the derivative of a sliding surface is derived as follows:

$$\begin{aligned}\dot\sigma(t) &= \sum_{i=1}^{9} \mu^i(x)\{[I + G_1 \Delta B(x, x_{\tau_x}, t)(G_1 \bar B^i)^{-1}](G_1 \bar B^i) w^i(t) \\ &\quad + \tilde W^i(t)^T \Phi(\rho) + \upsilon(\rho) + \varepsilon_\Omega^i(t)\}\end{aligned} \tag{38}$$

where $\tilde W^i(t) = W^i - \hat W^i(t)$.

Then, the following theorem for the operating point inside of $\|\sigma(t)\| = n_{\sigma 2}$ is proposed.

Theorem 3: Consider the same conditions as of Theorem 1 except that $\|\eta_2^i\|_F > p_\upsilon^i + h_\varepsilon^i$ and that the updating law (30) is applied to accomplish the learning term $\hat W^i(t)^T \Phi(\rho)$ with $F(\|\sigma(t)\|) = 1$ in (28a). Then $\sigma(t), u(t), \hat W^1(t), \ldots,$ and $\hat W^N(t)$ are UUB, and the system performance is obtained as follows:

$$\begin{aligned}P_a = \{&Z(t) \in \Re^{10} | 0 \le \|\sigma(t)\| \le p_{\max}, \\ &0 \le \|\tilde W^i(t)\|_F \le s^i, \qquad \text{for } 1 \le i \le 9\}\end{aligned} \tag{39}$$

where $p_{\max} = \max_{1\le i\le 9}(p^i)$, $s^i = \gamma^i W_m^i/(\gamma^i - \delta/2)$, $p^i = \sqrt{(p_1^i)^2 + p_2^i} - p_1^i, p_1^i = \{\varepsilon^i + (\|\eta_2^i\|_F - p_\upsilon^i - h_\varepsilon^i)/(\|\eta_1^i\|_F - \delta/2)\}/2$, and $p_2^i = \varepsilon^i(p_\upsilon^i + h_\varepsilon^i)/(\|\eta_1^i\| - \delta/2)$.

Proof: See Appendix B.

Remark 6: Because $p_\upsilon^i \ll h_\Omega^i(\rho)$, the comparison between $p_{\max}$ in (39) and $h_{\max}$ in (36) shows that the tracking performance, i.e., $\|\sigma(t)\|$, of the adaptive control is much smaller than that in robust control. However, a mere adaptive control often results in a transient response. In this situation, a robust control is first used to force the operating point to converge to an acceptable set and then an extra compensation of the uncertainties (i.e., adaptive control) is used to enhance system performance.

Remark 7: As $n_{\sigma 1} \ge \|\sigma(t)\| \ge n_{\sigma 2}$, the corresponding result can refer to our previous study [23]. In addition, the scalar function $F(\|\sigma(t)\|)$ can be designed as a vector function $F(\sigma(t))$ such that different channels possess different schemes of (29)

$$F(\sigma(t)) = \text{diag}\{f(|\sigma_1(t)|), f(|\sigma_2(t)|)\} \tag{40}$$

where $f(|\sigma_i(t)|)$, as shown at the bottom of the page.

V. Experiments and Discussion

A. Experimental Preliminaries

1) Tracking Mode: Two types of tracking modes are considered, namely 1) approach mode and 2) fine-tune mode. The purpose of the approach mode is to drive the CLWR to the neighborhood of the line-segments path. Then, the fine-tune mode is applied to force the CLWR to be the line-segments path (or as close as possible). It is well-known that the relative angle between the orientation of the CLWR and that of the line-segments path is the index for the desired steering angle θ_{1d}. Certainly, the CLWR in the left or right region of the line-segments path also affects the desired steering angle. However, the tracking mode for the left or right region is similar. For brevity, only the motion of the CLWR in the left region is depicted in Fig. 7. The content of large circle with dash-dotted line in Fig. 7 indicates the concept of the fine-tune mode. After the CLWR is in the region of the fine-tune mode, the tracking of line-segment path is illustrated, as in Fig. 8. To begin with, the turning angle δ_{i-1} of the $(i-1)$th segment is defined as the relative angle between the ith segment and the $(i-1)$th segment. The turning point p_{i-1} or turning

$$f(|\sigma_i(t)|) = \begin{cases} 0, & \text{as } |\sigma_i(t)| > n_{i\sigma 1} \\ 1, & \text{as } |\sigma_i(t)| < n_{i\sigma 2}, \quad i = 1, 2. \\ (n_{i\sigma 1} - |\sigma_i(t)|)/(n_{i\sigma 1} - n_{i\sigma 2}), & \text{otherwise} \end{cases}$$

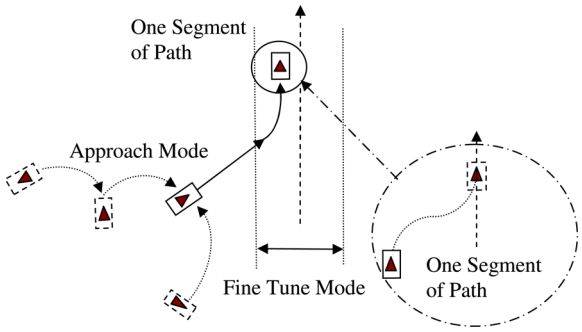

Fig. 7. Illustration of path tracking mode.

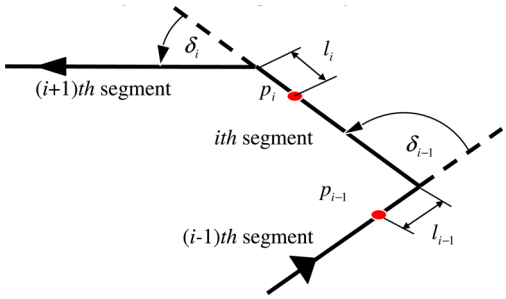

Fig. 8. Illustration of path tracking of line segments.

length l_{i-1} of the $(i-1)$th segment in Fig. 8 is represented as the point or the position starting to turn into the ith segment. Based on our analysis, the following relation $l_{i-1} = c_2(\delta_{i-1})^{c_1}$, where $c_1 = 0.5$, $c_2 = 42$ cm, and the unit of δ_{i-1} is radian, is employed to track a path of multiple line segments.

2) Strategy of Obstacle Avoidance: The strategy for the avoidance of static and dynamic obstacles is introduced. When a CLWR is faced with a staticobstacle or dynamic obstacle, the strategies can be simultaneously applied to avoid these obstacles. The strategy for the avoidance of a static obstacle in Fig. 9(a) is first described.

1) As the distance between the corresponding point of the CLWR and the obstacle (i.e., L_1) is smaller than $L_{1,\min}$, the CLWR starts the operation to avoid the corresponding obstacle. That is, the operation of the CLWR is in a mode of static obstacle avoidance. In addition, it is not limited only to one static obstacle.
2) As the minimum distance between the corresponding point of the CLWR and the obstacle (i.e., L_2) is greater than $L_{2,\min}$, then $\theta_{1d} = 0$ so that the CLWR moves in a straight line.
3) As $|\alpha - \beta| > 90°$, the operation of the CLWR returns to the path tracking mode.

Remark 8: Strategy 3) for the avoidance of a static obstacle is explained as follows. Based on the definitions of the angles α and β, if the CLWR is on the right-hand side of the obstacle and leaves away from it, i.e., $\alpha \leq 90°$ and $\beta = 180°$, then $|\alpha - \beta| > 90°$. Similarly, if the CLWR is on the left-hand side of the obstacle and leaves away from it, i.e., $\alpha \geq 90°$ and $\beta = 0°$, then $|\alpha - \beta| > 90°$. At this moment, the CLWR has avoided the obstacle and it should return to the path tracking mode.

Similarly, the strategy for the avoidance of a dynamic obstacle, as in Fig. 9(b), is depicted as follows:

1) As the value $\bar{y}$ of the CLWR is smaller than $y_{\min}$, the CLWR stops.
2) The CLWR starts to track the path when either of the following conditions is satisfied:
   a) $\bar{x} > x_{\text{depature}}$, where $\bar{x}$ denotes the distance between the intersection of the path and the center of the CLWR, departing from the intersection, and x_{depature} represents an assigned distance to prevent the CLWR from bumping against a dynamic obstacle;
   b) $\tilde{x} > x_{\text{arrival}}$, where $\tilde{x}$ stands for the distance between the intersection of the path and the center of the CLWR, arriving into the intersection, and x_{arrival} denotes an assigned distance to prevent the CLWR from bumping against a dynamic obstacle.

In the beginning, the images captured by two CCDs for a time interval (e.g., 2 s) are obtained to judge whether the visible area (or smart space) is in the presence of a static obstacle or dynamic obstacle. If the obstacle is static, the corresponding position (x, y) is input for the path planning to avoid this static obstacle. If the obstacle is dynamic, its position is estimated in every sampling interval (i.e., 260 ms) and input for the path planning to avoid the dynamic obstacle. In this paper, the corresponding parameters for (static and dynamic) obstacle avoidance are set as follows: $L_{1,\min} = 60$ cm, $L_{1,\min} = 60$ cm, $L_{2,\min} = 15$ cm, $x_{\text{departure}} = 20$ cm, $x_{\text{arrival}} = 60$ cm, and $y_{\min} = 60$ cm.

B. Experimental Results

From the very beginning, the performances of two motors are evaluated when the CLWR does not contact with the ground, i.e., CLWR is off ground. The coefficients of sliding surface (26) are set as $G_1 = \begin{bmatrix} 9.2 & 0 & 0.5 & 0 \\ 0 & 14.5 & 0 & 14.2 \end{bmatrix}$ and $G_2 = \begin{bmatrix} 0.5 & 0 & 0 & 0 \\ 0 & 3 & 0 & 0 \end{bmatrix}$. In other words, $\sigma_1(t) = 0.5\dot{\tilde{x}}_1(t) + 9.2\tilde{x}_1(t) + 0.5\int \tilde{x}_1(\tau)\, d\tau$ and $\sigma_2(t) = 14.2\dot{\tilde{x}}_2(t) + 14.5\tilde{x}_2(t) + 3\int \tilde{x}_2(\tau)\, d\tau$; they contain the eigenvalues $-0.0545, -18.3455$ and $-0.28829, -0.73284$, respectively. The control parameters of robust control are set as follows: $\eta_1^i = \text{diag}\{16.0, 35.0\}$, $\eta_2^i = \text{diag}\{1.0, 2.2\}$, $\varepsilon^i = 0.1$, and $\alpha^i = 0.2$. It indicates that the dynamics of a sliding surface possesses a low-pass feature to reduce the effect of the high-frequency component of the tracking error. A RBFNN with $L = 3^7 + 1 = 730$ is first employed to learn the system uncertainties; then, the environment uncertainty is reduced. In addition, control parameters are used in the robust control, and $\gamma^i = 0.01$ and $\beta^i = 15$ are selected for the updating law (30). The parameters $n_{\sigma 1} = 0.3$ and $n_{\sigma 2} = 0.8$ are applied to partition the robust control and adaptive control for the following experiments.

The experiments are divided into the following three cases: 1) to track a set of line segments with different initial poses of the CLWR; 2) to track the same path as in part 1) but with two static obstacles; and 3) to track the same path as in part 1) but with one static and one dynamic obstacle in the X-axis direction. The positions of two static obstacles with radius 25 cm are $(X, Y) = (-72.32, 259.48)$ and $(91.33, 295.31)$ cm, respectively. The path to be tracked is made up of five segments of straight line (i.e., the dash lines in Figs. 10 and 11). The coordinates of the five segments from the start point to the end point are $(-45, 0)$,

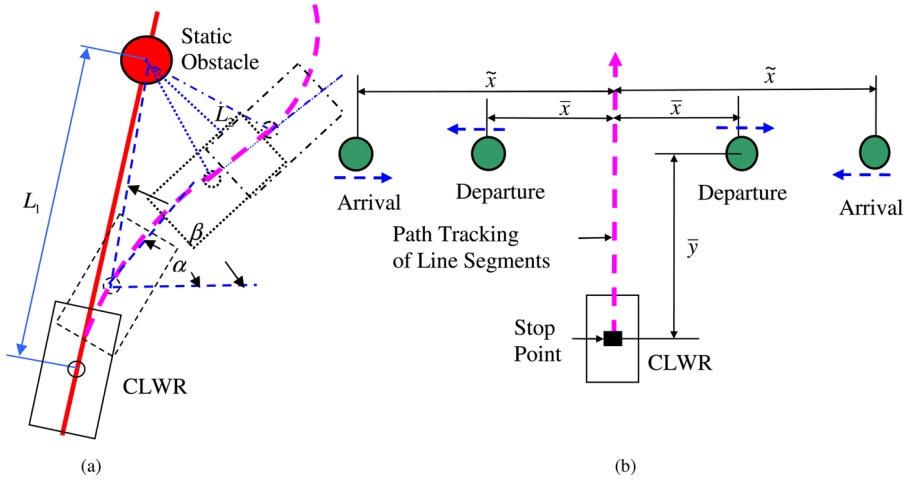

Fig. 9. Strategy for the avoidance of static and dynamic obstacles: (a) static obstacle; (b) dynamic obstacle.

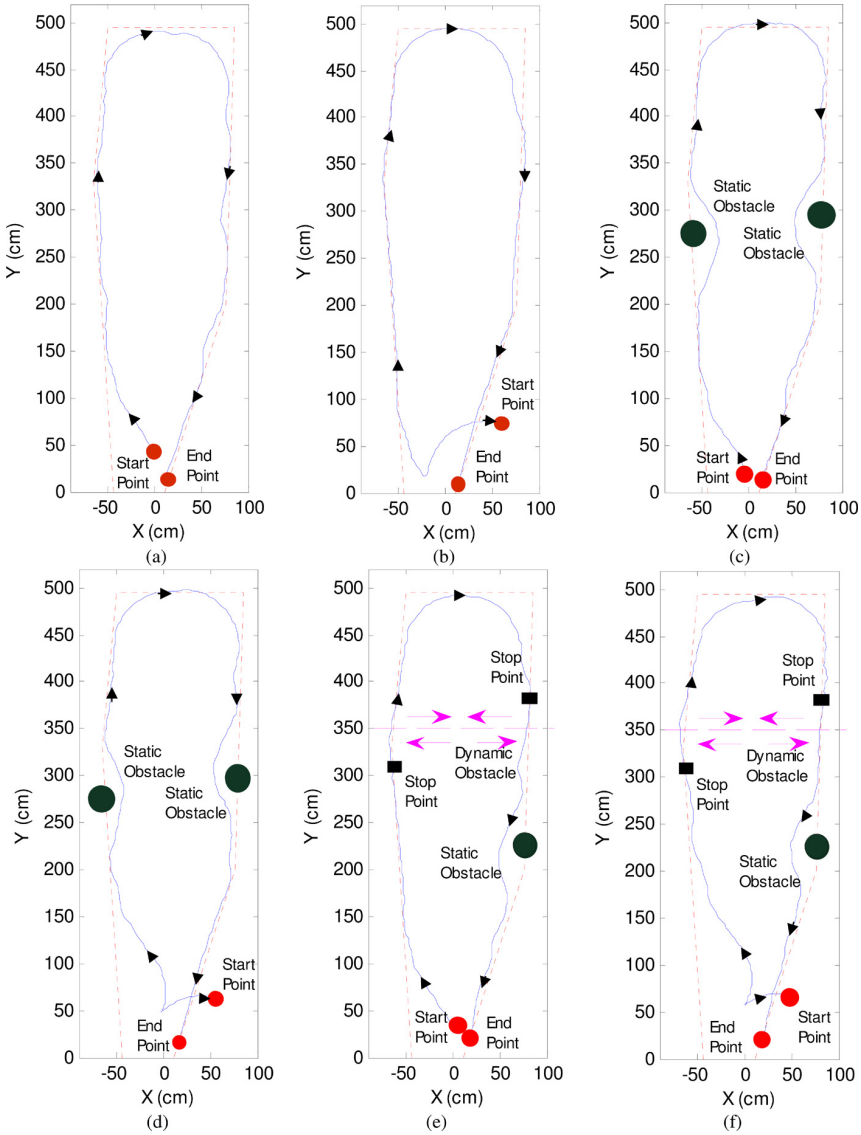

Fig. 10. Responses of the navigation for the IBSS-CLWR with $\nu_d = 28.6$ cm/s and different initial poses for the following six cases: (a) and (b), without obstacle; (c) and (d), two static obstacles; (e) and (f), one static obstacle and one dynamic obstacle.

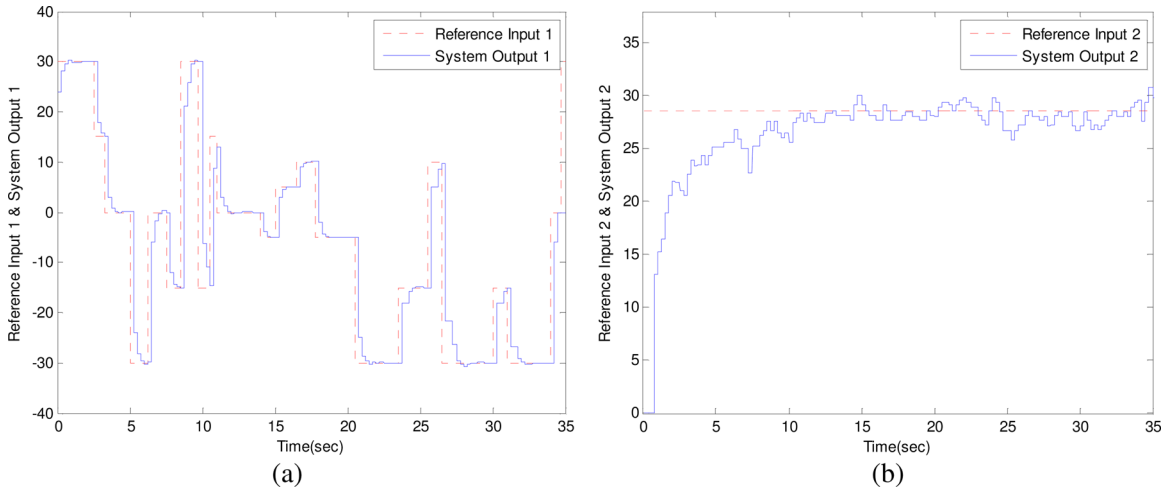

Fig. 11. Responses of the steering angle and translation velocity of Fig. 10(a): (a) front-wheel; (b) rear-wheel.

$(-65, 330)$, $(-50, 495)$, $(85, 495)$, $(75, 200)$, and $(10, 0)$ cm. Then, the corresponding responses of the aforementioned three cases are shown in Fig. 10 for $\nu_d = 28.6$ cm/s. The responses in the *neighborhood* of the overlap region, which is simultaneously visible by CCD1 and CCD2, e.g., $275 < Y < 325$ cm, are often in an unfavorable situation due to the discontinuity resulting from the pose estimation and the reduced quality of the image system. Because there always exists a minimum turning radius for a CLWR, the tracking performance in the third segment is inferior. In this situation, an omnidirectional wheeled robot (e.g., [24]) should be considered instead. Although the segments to be tracked are in the periphery of smart space with reduced quality in pose estimation, the performances in Fig. 10 are still acceptable to confirm the usefulness of our control system. In addition, the responses of the steering angle and the translation velocity of Fig. 10(a) by using the FNAC are shown in Fig. 11, which are apparently acceptable responses.

Before comparing the results obtained by executing our proposed FNAC with that obtained by using PID control, the parameters of PID control are chosen such that the off-ground CLWR has good enough performance. By comparing the performance, as shown in Fig. 10(a) and (c) obtained by CLWR, with the performance shown in Fig. 12 with PID control with the same case, it appears that PID control is inferior to the CLWR. Although in Fig. 12 it has a total delay between 210 and 260 ms and we have a sound result by using PID control, it will fail if the time delay of the IBSS-CLWR is changed too much. For instance, a total time-varying delay in the range of 260∼310 ms will navigate the CLWR outside of the visible area of CCD1 and CCD2, and a total time-varying delay in 310∼360 ms will result in a negative phase margin. However, our proposed control can survive to accomplish the desired goal [23]. These features are verified by our experiments. Because the bandwidth of the IBSS-CLWR is constrained by the sampling rate, its motion becomes slower as the larger sampling time is used. For simplicity, these results are omitted. In summary, the robustness of PID control is worse than that of our proposed control. If the monitoring region is wide, the number of the CCD cameras should be increased or the active CCD camera should be considered.

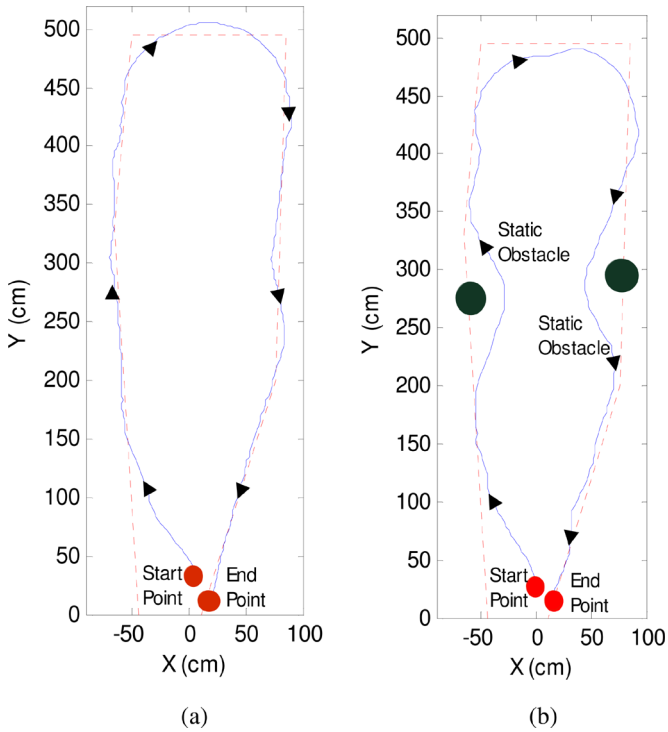

Fig 12. Responses of PID control for the cases of Fig. 10(a) and (c): (a) without obstacle; (b) two static obstacles.

VI. Conclusion

Nine subsystems without delay are developed from the step responses of the CLWR with nine specific conditions, which are also assigned as the premise variables for the fuzzy rule. To our best knowledge, we believe that it is the first time in fuzzy modeling that the model has been developed from the CLWR step responses with various conditions. Meanwhile, the transmission delays of the input and output signals passing through the IN and WLAN, the image processing time, and the total calculation time in the control algorithm are estimated. Eventually, the fuzzy delay modeling of an IBSS-CLWR is achieved.

Then, a suitable fuzzy reference model is applied to shape the response of the closed-loop system. Based on these operations, our proposed FNAC is designed without the constraint on the upper bound of the time-varying delay for the input of an IBSS-CLWR. However, the uncertainties caused by the fuzzy-model error and the interactions among subsystems must be relatively bounded, and the stabilizing conditions of every transformed delay-free subsystem must be satisfied. Although the line segments to be tracked are on the periphery of smart space, and incurring quality in the pose estimation, our proposed control system provides satisfactory performance in path tracking and obstacle avoidance. If the delay of the controlled system is beyond range, the traditional control (e.g., robust control, PID control) often fails due to the retarded navigation of the CLWR and the existence of a negative phase margin. If the monitoring area is wide, the number of the CCD cameras should be increased or the active CCD camera should be considered.

APPENDIX A: PROOF OF THEOREM 1

Define the following Lyapunov function:

$$V = \sigma^T \sigma/2 > 0, \text{ as } \sigma \neq 0. \tag{A1}$$

Taking the time derivative of (A1) and assuming that $\dot{V} \leq -\delta V$ where $\delta > 0$ gives

$$\dot{V}_{\text{asy}} = \sigma^T \dot{\sigma} + \delta \sigma^T \sigma/2 \tag{A2}$$

where $\dot{V}_{\text{asy}} = \dot{V} + \delta V$. Substituting (28b), (34), and (35) into (A2) yields

$$\begin{aligned}
\dot{V}_{\text{asy}} &\leq \sigma^T \left\{ \sum_{i=1}^{9} \mu^i \left[\frac{-(I + G_1 \Delta B (G_1 \bar{B}^i)^{-1})}{\sqrt{2} - \alpha^i} \right.\right. \\
&\qquad \left.\left. \cdot \left(\eta_1^i \sigma + \frac{\eta_2^i \sigma}{\|\sigma\| + \varepsilon^i} \right) + \Omega^i + \varepsilon_\Omega^i \right] + \frac{\delta \sigma}{2} \right\} \\
&\leq - \sum_{i=1}^{9} \frac{\mu^i \left(\|\eta_1^i\|_F - \delta/2 \right) \|\sigma\|}{\|\sigma\| + \varepsilon^i} \\
&\qquad \times \left\{ \|\sigma\| (\|\sigma\| + \varepsilon^i) + \frac{\|\eta_2^i\|_F}{(\|\eta_1^i\|_F - \delta/2)} \|\sigma\| \right. \\
&\qquad \left. - \frac{h_\Omega^i + h_\varepsilon^i}{(\|\eta_1^i\|_F - \delta/2)} (\|\sigma\| + \varepsilon^i) \right\} \\
&\leq - \sum_{i=1}^{9} \mu^i (\|\eta_1^i\|_F - \delta/2) \|\sigma\| H^i(\|\sigma\|) / (\|\sigma\| + \varepsilon^i)
\end{aligned} \tag{A3}$$

where $H^i(\|\sigma\|) = \|\sigma\|^2 + 2h_1^i \|\sigma\| - h_2^i$. When $\|\sigma\| \geq h_{\max}$, the inequalities $H^i(\|\sigma\|) \geq 0$ for $i = 1, 2, \ldots, 9$, are satisfied. Then, outside of the domain P_r in (36a), $\dot{V}_{\text{asy}} \leq 0$ (or $\dot{V} \leq -\delta V$) is achieved. Hence, the signal σ exponentially converges into the domain P_r. Finally, from (27) and (28) u is UUB. Q.E.D.

APPENDIX B: PROOF OF THEOREM 3

Similarly, the arguments of variable are omitted. Define the following Lyapunov function:

$$\begin{aligned}
V &= \sigma^T \sigma/2 + \sum\nolimits_{i=1}^{9} \mu^i \text{tr}\{(\tilde{W}^i)^T \tilde{W}^i\}/(2\beta^i) \\
&= Z^T R Z > 0, \qquad \text{as } \sigma \neq 0 \text{ or } \tilde{W}^i \neq 0
\end{aligned} \tag{B1}$$

where $R = \text{Diag}[\,1/2 \quad \mu^1/(2\beta^1) \quad \ldots \quad \mu^9/(2\beta^9)\,] > 0 \in \Re^{10 \times 10}$, tr$\{\}$ stands for the trace operator, and $\text{tr}\{A\} = \sum_{i=1}^{n} a_{ii}$, where $A \in \Re^{n \times n}$. Similarly, taking the time derivative of (B1), assuming that $\dot{V} \leq -\delta V$ where $\delta > 0$ and using (28) and (37), yields

$$\begin{aligned}
\dot{V}_{\text{asy}} &= \dot{V} + \delta V \\
&\leq \sigma^T \left\{ \sum_{i=1}^{9} \mu^i \left[\frac{-(I + G_1 \Delta B (G_1 \bar{B}^i)^{-1})}{\sqrt{2} - \alpha^i} \left(\eta_1^i \sigma + \frac{\eta_2^i \sigma}{\|\sigma\| + \varepsilon^i} \right) \right.\right. \\
&\qquad \left.\left. + (\tilde{W}^i)^T \Phi + \upsilon^i + \varepsilon_\Omega^i \right] + \frac{\delta \sigma}{2} \right\} \\
&\quad - \sum_{i=1}^{9} \mu^i tr\{(\tilde{W}^i)^T (\beta^i \Phi \sigma^T - \gamma^i \hat{W}^i)\}/\beta^i \\
&\quad + \delta \sum_{i=1}^{9} \mu^i tr\{(\tilde{W}^i)^T \tilde{W}^i\}/(2\beta^i) \\
&= \sigma^T \left\{ \sum_{i=1}^{9} \mu^i \left[\frac{-(I + G_1 \Delta B (G_1 \bar{B}^i)^{-1})}{\sqrt{2} - \alpha^i} \left(\eta_1^i \sigma + \frac{\eta_2^i \sigma}{\|\sigma\| + \varepsilon^i} \right) \right.\right. \\
&\qquad \left.\left. + (\tilde{W}^i)^T \Phi + \upsilon^i + \varepsilon_\Omega^i \right] + \frac{\delta \sigma}{2} \right\} \\
&\quad + \sum_{i=1}^{9} \mu^i tr\{(\tilde{W}^i)^T \gamma^i (W^i - \tilde{W}^i) + \delta (\tilde{W}^i)^T \tilde{W}^i/2\}/\beta^i \\
&\leq - \sum_{i=1}^{9} \frac{\mu^i \left(\|\eta_1^i\|_F - \delta/2 \right) \|\sigma\|}{\|\sigma\| + \varepsilon^i} \\
&\quad \times \left\{ \|\sigma\| (\|\sigma\| + \varepsilon^i) + \frac{\|\eta_2^i\|_F}{\left(\|\eta_1^i\|_F - \delta/2 \right)} \|\sigma\| \right. \\
&\quad \left. - \frac{p_\upsilon^i + h_\varepsilon^i}{\left(\|\eta_1^i\|_F - \delta/2 \right)} (\|\sigma\| + \varepsilon^i) \right\} \\
&\quad - \sum_{i=1}^{9} \mu^i \left\{ \frac{(\gamma^i - \delta/2) \|\tilde{W}^i\|_F^2 - \gamma^i W_m^i \|\tilde{W}^i\|_F}{\beta^i} \right\} \\
&\leq - \sum_{i=1}^{9} \mu^i \left\{ \frac{(\|\eta_1^i\|_F - \delta/2) \|\sigma\| P^i(\|\sigma\|)}{\|\sigma\| + \varepsilon^i} \right. \\
&\qquad \left. + \frac{(\gamma^i - \delta/2) \|\tilde{W}^i\|_F Q^i(\|\tilde{W}^i\|_F)}{\beta^i} \right\}
\end{aligned} \tag{B2}$$

where $P^i(\|\sigma\|) = \|\sigma\|^2 + 2p_1^i\|\sigma\| - p_2^i$, $Q^i(\|\tilde{W}^i\|_F) = \|\tilde{W}^i\|_F - s^i$. When $\|\sigma\| \geq p_{\max}$ and $\|\tilde{W}^i\|_F \geq s^i$ for $i = 1, 2, \ldots, 9$ the inequalities $P^i(\|\sigma\|) \geq 0$ and $Q^i(\|\tilde{W}^i\|_F) \geq 0$ for $i = 1, 2, \ldots, 9$, are obtained. Then, outside of the domain P_a in (39a) makes $\dot{V}_{\text{asy}} \leq 0$(or $\dot{V} \leq -\delta V$). Hence, the signal Z exponentially converges into the domain P_a. Finally, from (27) and (28), u is UUB. Q.E.D.

ACKNOWLEDGMENT

The authors wish to thank the anonymous reviewers for their constructive suggestions toward the improvement of the presentation of this paper.

REFERENCES

[1] F. Amigoni, N. Gatti, C. Pinciroli, and M. Roveri, "What planner for ambient intelligence applications?" *IEEE Trans. Syst., Man, Cybern.–A: Syst. Humans*, vol. 35, no. 1, pp. 7–21, Jan. 2005.

[2] F. Zhao and L. Guibas, *Wireless Sensor Networks: An Information Processing Approach*. Amsterdam, The Netherlands: Elsevier, 2005.

[3] C. L. Hwang, N. W. Chang, and S. Y. Han, "Fuzzy decentralized sliding-mode control of car-like mobile robots in a distributed sensor-network space," in *Proc. 3rd Int. Conf. Comput. Intell. Robot. Auton. Syst. (ICRAS),* Singapore, Dec. 13–16, 2005.

[4] S. Se, D. G. Lowe, and J. J. Little, "Vision-based global localization and mapping for mobile robots," *IEEE Trans. Robot.*, vol. 21, no. 3, pp. 364–375, Jun. 2005.

[5] S. X. Yang and Q. H. Meng, "Real-time collision-free motion planning of a mobile robot using a neural dynamics-based approach," *IEEE Trans. Neural Netw.*, vol. 14, no. 6, pp. 1541–1552, Nov. 2003.

[6] T. H. S. Li and S. J. Chang, "Fuzzy target tracking control of autonomous mobile robots by using infrared sensors," *IEEE Trans. Fuzzy Syst.*, vol. 12, no. 4, pp. 491–501, Aug. 2004.

[7] I. Baturone, F. J. Moreno-Velo, S. Sanchez-Solano, and A. Ollero, "Automatic design of fuzzy controllers for car-like autonomous robots," *IEEE Trans. Fuzzy Syst.*, vol. 12, no. 4, pp. 447–465, Aug. 2004.

[8] P. Carinena, C. V. Regueiro, A. Otero, J. Bugarin, and S. Barro, "Landmark detection in mobile robotics using fuzzy temporal rules," *IEEE Trans. Fuzzy Syst.*, vol. 12, no. 4, pp. 423–435, Aug. 2004.

[9] R. J. Anderson and M. W. Spong, "Bilateral control of teleoperators with time delay," *IEEE Trans. Autom. Control*, vol. 34, no. 5, pp. 494–501, Oct. 1989.

[10] S. Munir and W. J. Book, "Internet-based teleoperation using wave variables with prediction," *IEEE/ASME Trans. Mechatronics*, vol. 7, no. 2, pp. 124–133, Apr. 2002.

[11] K. R. Lee, J. H. Kim, E. T. Jeung, and H. B. Park, "Output feedback robust control of uncertain fuzzy dynamic systems with time-varying delay," *IEEE Trans. Fuzzy Syst.*, vol. 8, no. 6, pp. 657–664, Dec. 2000.

[12] B. S. Chen, Y. S. Yang, B. K. Lee, and T. H. Lee, "Fuzzy adaptive predictive flow control of ATM network traffic," *IEEE Trans. Fuzzy Syst.*, vol. 11, no. 4, pp. 568–581, Aug. 2003.

[13] F. Mazenc, S. Mondi, and S. I. Niculescu, "Global asymptotic stabilization for chains of integrators with a delay in the input," *IEEE Trans. Autom. Control*, vol. 48, no. 1, pp. 57–63, Jan. 2003.

[14] Y. A. Fiagbedzi and A. E. Pearson, "Feedback stabilization of linear autonomous time lag systems," *IEEE Trans. Autom. Control.*, vol. AC-31, no. 9, pp. 847–855, Sep. 1986.

[15] J. S. Luo, P. P. J. Van Den Bosch, S. Weiland, and A. Goldenberge, "Design of performance robustness for uncertain linear systems with state and control delays," *IEEE Trans. Autom. Control*, vol. 43, no. 11, pp. 1593–1612, Nov. 1998.

[16] J. P. Richard, "Time-delay systems: An overview of some recent advances and open problems," *IFAC J. Autom.*, vol. 39, pp. 1667–1694, 2003.

[17] H. Fazelinia, R. Sipahi, and N. Olgac, "Stability robustness analysis of multiple time-delayed systems using 'building block' concept," *IEEE Trans. Autom. Control*, vol. 52, no. 5, pp. 799–811, May 2007.

[18] M. R. Stojic, M. S. Matijevic, and L. S. Draganovic, "A robust Smith predictor modified by internal models for integrating process with dead time," *IEEE Trans. Autom. Control*, vol. 46, no. 8, pp. 1293–1298, Aug. 2001.

[19] J. Q. Huang, F. L. Lewis, and K. Liu, "Neural-network predictive control for nonlinear dynamic systems with time-delay," *IEEE Trans. Neural Netw.*, vol. 14, no. 2, pp. 377–389, Mar. 2003.

[20] S. Haykin, *Neural Networks—A Comprehensive Foundation*, 2nd ed. Englewood Cliffs, NJ: Prentice-Hall, 1999.

[21] C. L. Hwang, "Neural-network-based variable structure control of electro-hydraulic servosystems subject to huge uncertainties without the persistent excitation," *IEEE/ASME Trans. Mechatronics*, vol. 4, no. 1, pp. 50–59, Mar. 1999.

[22] R. M. Sanner and J.-J. E. Slotine, "Gaussian networks for direct adaptive control," *IEEE Trans. Neural Netw.*, vol. 3, no. 6, pp. 837–863, May 1992.

[23] C. L. Hwang, "A novel Takagi–Sugeno-based robust adaptive fuzzy sliding-mode controller," *IEEE Trans. Fuzzy Syst.*, vol. 12, no. 5, pp. 676–687, Oct. 2004.

[24] R. L. Williams, II, B. E. Carter, P. Gallina, and G. Rosati, "Dynamic model with slip for wheeled omnidirectional robots," *IEEE Trans. Robot. Autom.*, vol. 18, no. 3, pp. 285–293, Jun. 2002.

Chih-Lyang Hwang (M'98) received the B.E. degree in aeronautical engineering from Tamkang University, Tamsui, Taipei Hsien, Taiwan, R.O.C., in 1981, the M.E. and Ph.D. degrees in mechanical engineering from Tatung Institute of Technology, Taipei, Taiwan, in 1986 and 1990, respectively.

From 1990 to 2006, he was with the Department of Mechanical Engineering, Tatung Institute of Technology (Tatung University), where from 1996 to 2006, he was a Professor of mechanical engineering, engaged in teaching and research in the area of servo control and control of manufacturing systems and robotic systems. During 1998–1999, he was a Research Scholar at George W. Woodruf School of Mechanical Engineering, Georgia Institute of Technology, Atlanta. From 2003 to 2006, he was on the committee of the Automation Technology Program of the National Science Council of Taiwan. Since 2006, he has been a Professor in the Department of Electrical Engineering, Tamkang University. He is the author or coauthor of more than 100 journal and conference papers. His current research interests include navigation of mobile robots, fuzzy (or neural network) modeling and control, variable structure control, robotics, visual tracking systems, network-based control, and distributed sensor networks.

Prof. Hwang was on the technical committee of IEEE IECON02. He was the recipient of numerous awards including the Excellent Research Paper Award from the National Science Council of Taiwan and Hsieh-Chih Industry Renaissance Association of Tatung Company.

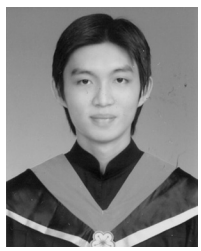

Li-Jui Chang received the B.E. and M.E. degrees in mechanical engineering from Tatung University, Taipei, Taiwan, R.O.C., in 2005 and 2006, respectively.

He is currently with Marketech International Corporation, Taipei. His current research interests include navigation of mobile robots and fuzzy control.